S-Band Maser Phase Delay Stability Tests

J. M. Urech, F. Alcazar, J. Galvez, and A. Rius
Madrid Deep Space Station

C. A. Greenhall
TDA Engineering Office

This article summarizes the results of the S-band traveling-wave maser phase delay stability measurements performed at DSS 62. These tests were required for the Pioneer-Venus wind experiment.

I. Introduction

This article summarizes the results of the S-band traveling-wave maser phase delay stability measurements performed at DSS 62. In conjunction with earlier group delay measurements, this article completes the group and phase delay measurements required for the Pioneer-Venus 78 wind experiment.

All tests were performed for the entire S-band maser passband, which includes the 5-MHz passband, from 2290 to 2295 MHz, used in the entry probe wind experiment. This experiment requires that the phase delay variation be less than 1 deg over a 2-MHz passband (2291 to 2293 MHz).

II. Test Configuration

All the tests were performed on the declination (dec) room maser. Figure 1 shows the physical location of test equipment. As can be seen, most of this was installed in the empty part of receiver rack 9.

Figure 2 is the test configuration schematic. To have a phase delay difference of less than 180 deg between test and reference paths, a delay line was fabricated locally. This consisted of about 38 meters of soft line encapsulated in a plastic box and insulated thermally.

III. Phase Delay Stability Versus Maser Parameters

Phase delay variation over a given frequency band is defined as max $\Delta\phi(f)$ - min $\Delta\phi(f)$, where $\phi(f)$ is the phase delay versus frequency curve, $\Delta\phi(f)$ is the change in $\phi(f)$ due to some internal or environmental change, and the max and min are over all f in the band. Notice that if the $\phi(f)$ curve simply moves parallel to itself, the phase delay variation is zero, since $\Delta\phi(f)$ is constant. If the phases of the signals from all Pioneer-Venus probes are shifted by the same amount, no harm is done because the phases are differenced.

Variations of five maser parameters were simulated employing the same method used in the group delay stability measurements (see Table 1).

The expected variations were taken from the technical manuals of the corresponding power supplies and checked

against actual variations for periods of about 24 hours. The scale factor is the ratio between the simulated and the expected parameter variations. This must be taken into account when estimating the expected phase delay stability.

A. Results

Figures 3 through 7 are copies of the actual curves obtained while performing the above tests. Table 2 summarizes the test results.

As shown, two sets of measurements were performed (Figs. 3 through 7 correspond to set No. 2) with the dispersion between both being 1.5 deg. This is more than acceptable taking into account the different factors involved.

The variations were measured for a passband of 40 MHz (2265 to 2305 MHz) as well as for the passband of interest in the probe wind experiment (2290 to 2295 MHz). They should be divided by the corresponding scale factor to obtain the expected variations.

B. Coherence with Group Delay Stability Results

By calculating the group delay stability from the data obtained for phase delay stability and comparing it with the data derived from measuring the group delay stability directly, a reasonable coherency may be obtained between both group and phase delay stability measurements. The relationship between group delay stability and phase delay stability is given by

$$\overline{\Delta\tau} = \frac{1}{2\pi B} |\Delta\phi_1 - \Delta\phi_2|$$

where

$\overline{\Delta\tau}$ = group delay stability from phase delay stability data

B = width of passband

$\Delta\phi_1$ and $\Delta\phi_2$ = phase delay differences in both extremes of the passband, considering their signs

The value of $\overline{\Delta\tau}$ may be derived for all parameter variations and compared with $\Delta\tau$, the group delay stability measured earlier. Figure 8 details the result of this comparison for the 40-MHz passband. It can be seen that the difference is less than 0.28 ns except for bandwidth current, where the difference is less than 1.07 ns.

C. Estimation of Phase Delay Stability Versus Room Temperatures

Due to the heavy tracking load, it was not possible to check the phase delay stability versus dec and control room temperatures. However, based on the coherency of results obtained, it is possible to derive from Eq. 1 the phase delay stability $|\Delta\phi_1 - \Delta\phi_2|$ from the group delay stability $\Delta\tau$ measured earlier. See Table 3.

IV. Stability Versus Antenna Orientation

The appropriate range of antenna movement to simulate the possible earth magnetic field variation (due to DSS 43 antenna position changes) during the entry probe wind experiment was estimated using the earth magnetic field model of Lang (Ref. 1):

$B_r = (2m \cos\theta)/R$ radial component

$B_\theta = (m \sin\theta)/R^3$ local meridian component

$B_\phi = 0$ local parallel component

where

$m = 8.1 \times 10^{25}$ gauss $\times$ cm^3

$R = 6.37 \times 10^8$ cm

θ = 50 deg for DSS 62 and 125 deg for DSS 43

From the above we found that the magnitude of the earth's magnetic field for DSS 62 is 0.47 gauss and its elevation angle is 59 deg. For DSS 43 the magnitude is 0.43 gauss. Therefore, by moving the DSS 62 antenna from the az = 0 deg, el = 59 deg position (HA = 0 deg, dec = 72 deg), where the maser magnetic field is perpendicular to the earth's magnetic field, to az = 180 deg, el = 40 deg (HA = 0 deg, dec = 340 deg), where both magnetic fields are parallel, it is possible to simulate a variation larger than that expected in the PV wind experiment. In addition, it should be noted that the earth's magnetic field at DSS 62 is slightly greater than at DSS 43.

Although during the actual test the antenna could only be moved from HA = 0 deg, dec = 70 deg to HA = 0 deg, dec = 360 deg due to safety reasons (personnel and test equipment in dec room), the above reasoning is still valid.

A. Results

Figure 9 illustrates the stability versus antenna orientation results. The antenna movement sequence was: Zenith (Z) → dec 70 deg → Zenith (Z') → dec 360 deg → Zenith (Z'').

It should be noted that it is quite impossible to tie down all the test equipment and cables so that they do not move during the antenna movement. Because of this, after multiple tests

that proved that for very small equipment and cable movements the phase delay may vary about 5 deg, we conclude that the differences between the curves shown in Fig. 9 for all zenith and dec 70-deg positions may be due to slight movements of the set-up components.

From the above it may be asserted that phase delay stability is better than 25 deg for the entire maser passband, 40 MHz, and better than 5 deg for the 5-MHz passband of interest here.

The reason for the different shape of the curves in Figs. 3 through 7 and the curve in Fig. 9 was a maser klystron change in between.

V. Long-Term Stability

The long-term stability of the maser phase delay was checked during periods of 8 hours. The test configuration was the one detailed in Fig. 2 except for the X-Y plotter. This was replaced by a strip chart recorder HP 7100.

During the warmup period of the test equipment, the phase delay drifted considerably. Moreover, for more than 6 hours after this period, the phase delay drifted continuously at a rate of 2 deg per hour.

To check that the phase delay drift observed during the first hour and a half was due to the test equipment warming up, we performed an additional test in which we replaced the maser by a soft line of the proper length. Under these conditions, all the drift should be due only to the test equipment (cables included). Results showed the same considerable drift during the first hour and a half. For about 6 hours after that, no appreciable drift was observed.

The conclusion of these long-term stability tests is that a phase delay drift of about 2 deg per hour can be expected.

VI. Conclusions

A. General

Considering the scale factors, one may infer from Table 2 that the parametric variation yielding the largest phase delay instability (in the 5-MHz passband) is the liquid HE temperature (vapor pressure gauge). The same result was obtained when measuring the group delay stability. Nevertheless, this phase instability is only about 0.16 deg. The root-sum-square (RSS) of the phase instabilities due to all parametric variations is 0.17 deg.

As far as room temperatures are concerned (Table 3), that of the dec room is the one yielding the highest phase delay instability, about 0.27 deg.

The RSS of all phase instabilities from Tables 2 and 3 is 0.32 deg, and the linear sum is 0.58 deg.

From the antenna movement tests (Table 4) it may be seen that the instability in the 5-MHz passband is better than 5 deg. It should be remembered that the simulated antenna movement represents almost a complete range of interaction between the maser and earth magnetic fields (from perpendicular to parallel position). The actual antenna movement during the 90-minute wind experiment will be 22.5 deg in hour angle. Hence, the change in the angle α between the magnetic fields of the earth and the maser is less than 22.5 deg. Assuming that the phase delay variation V is proportional to the change in cos α we have

$$V < 5 \text{ deg } \left(22.5 \frac{\pi}{180}\right) < 2 \text{ deg}$$

This bound corresponds to a 4-m error in the difference of probe position components over 90 minutes (0.74 deg over 1000 seconds) measured by the Goldstone-Canberra baseline. The requirement is for $<$ 1 deg over 1000 seconds, which is met. In addition, the wind experiment is intended to measure probe *velocities*. Since error Δv in the difference of probe velocity components is proportional to dV/dt, the largest that Δv can get is 4 m/5400 s = 0.00074 m/s, a negligible error. The position error is gradually accumulated over the whole 90-minute period. The same reasoning applies to the long-term drift discussed in Section V.

B. Curve Analysis

When comparing Figs. 3 through 5 with Figs. 6 through 7 it was observed that, while the curves in the first figures were rather parallel throughout the passband, the curves in Figs. 6 and 7 appear to "rotate" (or change slopes) near the DSN bandwidth (2285 to 2305 MHz) around which the maser klystron is tuned. This may be explained by using the Leflang model for the phase-versus-frequency maser characteristic, given in degrees by (Ref. 2)

$$\phi(f) = 6.56 \sum_{i=1}^{2} G_i \frac{2(f - f)/\Delta f_L}{1 + \left[2(f - f_i)/\Delta f_L\right]^2}$$

where G_i and f_i are the gain in dB and the central frequency of the i^{th} section, and Δf_L is the maser material resonance line width.

Assuming $\Delta f_L >> f - f_i$ we have

$$\phi(f) \approx 6.56 \sum_{i=1}^{2} G_i \left[\frac{2(f-f_i)}{\Delta f_L} - \frac{8(f-f_i)^3}{(\Delta f_L)^3} \right]$$

To first approximation,

$$\phi(f) \approx 6.56 \sum_{i=1}^{2} G_i \frac{2(f-f_i)}{\Delta f_L}$$

$$= \frac{13.12}{\Delta f_L} (G_1 + G_2) \left(f - \frac{G_1 f_1 + G_2 f_2}{G_1 + G_2} \right)$$

This expression is a straight line with its slope proportional to $G_1 + G_2$ and the intersection with the frequency axis being the gain-weighted mean of the central frequencies of the two sections. Hence, those parametric variations that mainly affect the f_1 and f_2 position (such as beam and reflector voltages and bandwidth control current) will yield rather parallel curves. On the other hand, those affecting $G_1 + G_2$, such as gain control voltage and cryogenic temperature (vapor pressure gauge), will give curves with different slopes and rotating around a zone determined by the klystron tuning.

As for the shape of curves in Fig. 9, the predominant effect for the dec 360-deg curve is the total gain while for the dec 70-deg curve it is the f_1, f_2 positions.

VII. Instability due to Cross-Head Modulation

During one set of measurements, the cross-head modulation effect appeared for a short period of time and has been reflected in Fig. 10. This instability has the same shape as that observed while measuring the group delay stability. The stability may be estimated at less than 5 deg and may be of some importance, if present. The shape of this curve can also be explained due to the rapid and opposite gain variations caused by the cross-head modulation effect.

References

1. Lang, K. R., *Astrophysical Formulae*, Springer-Verlag, Berlin, 1974.
2. Leflang, J. G., *Maser Development*, JPL Technical Report 32-1526, Vol. 15, pp. 92-95. Jet Propulsion Laboratory, Pasadena, Calif., 1973.

Table 1. Test conditions

Parameter	Simulated variation	Expected variation	Scale factor
Beam voltage	± 5 V	< 0.75 V	13.4
Reflected voltage	± 2 V	< 0.1 V	40
Bandwidth control current	± 1 mA	< 50 A	40
Gain control current	± 3 mA	< 50 A	120
Liquid helium temperature	1.3 N/cm^2 = 2 lb/in^2 (VPG)	0.4 N/cm^2 = 0.58 lb/in^2	3.2

Table 2. Results of parametric study

Parameter	Simulated variation	Measured phase delay variation for a 40-MHz passband, deg		Measured phase delay variation for a 5-MHz passband, deg		Scale factor
		Set 1	Set 2	Set 1	Set 2	
Beam voltage	± 5 V	7	6	< 0.5	0.5	13.4
Reflected voltage	± 2 V	9	8.5	2	0.5	40
Bandwidth control current	± 1 mA	2	2	0.5	1	40
Gain control current	± 3 mA	2	2.5	< 0.5	< 0.5	120
Liquid helium temperature	1.3 N/cm^2 = 2 lb/in^2	5	5	< 0.5	0.5	3.2

Table 3. Estimated phase delay stability versus room temperatures

Parameter	Simulated variation	Expected variation	Peak-to-peak variation of group delay, ns	Estimated phase delay stability, deg	
				B=40 MHz	B=5 MHz
Dec room temperature	1.7°C	1.7°C	0.3	2.1	0.27
Control room temperature	1.7°C	0.6°C	0.2	1.4	0.18

Table 4. Phase delay stability versus antenna orientation

Passband, MHz	Measured phase delay stability, deg
40 MHz (2265-2305 MHz)	Better than 25
5 MHz (2290-2295 MHz)	Better than 5

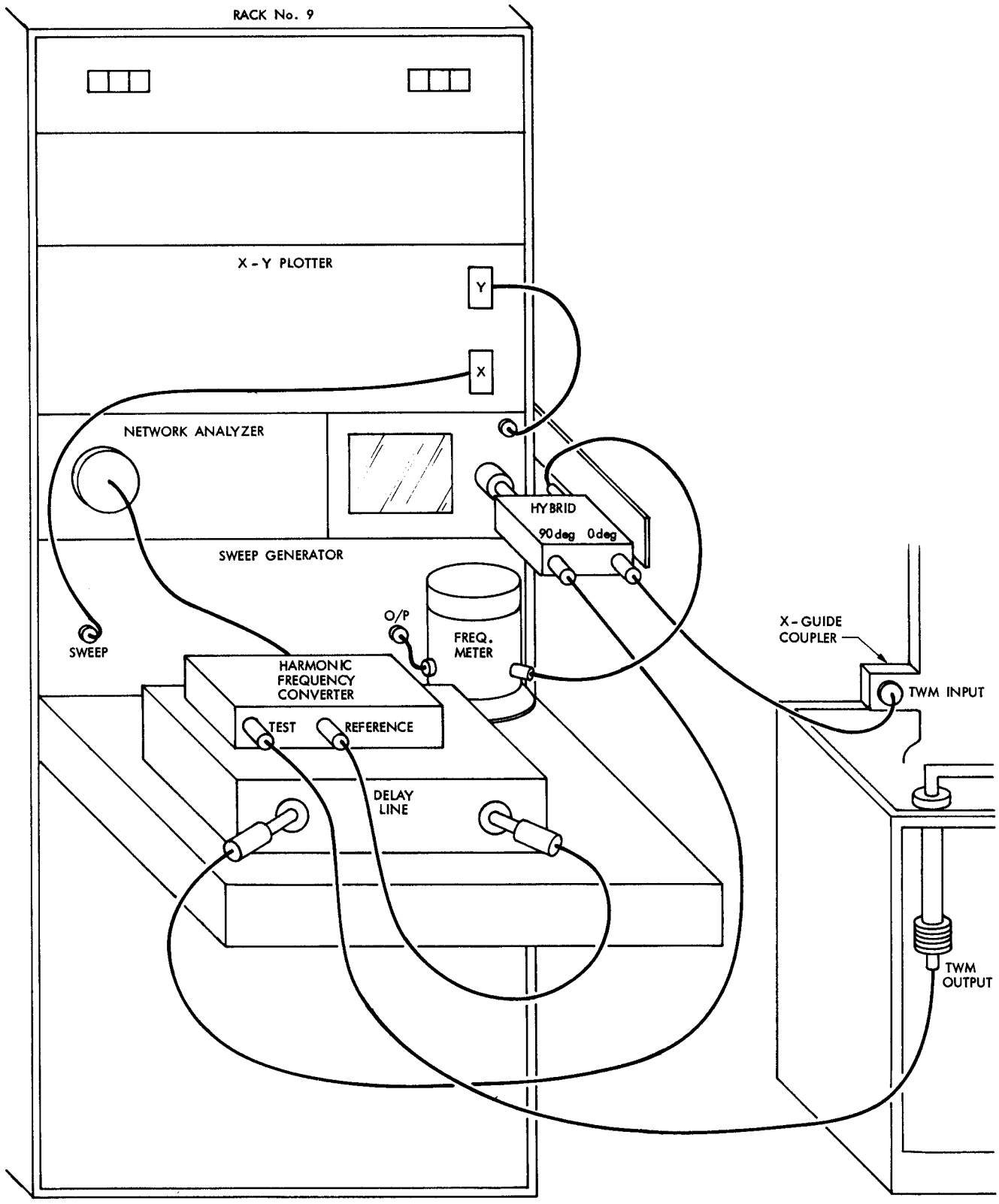

Fig. 1. Test equipment physical location

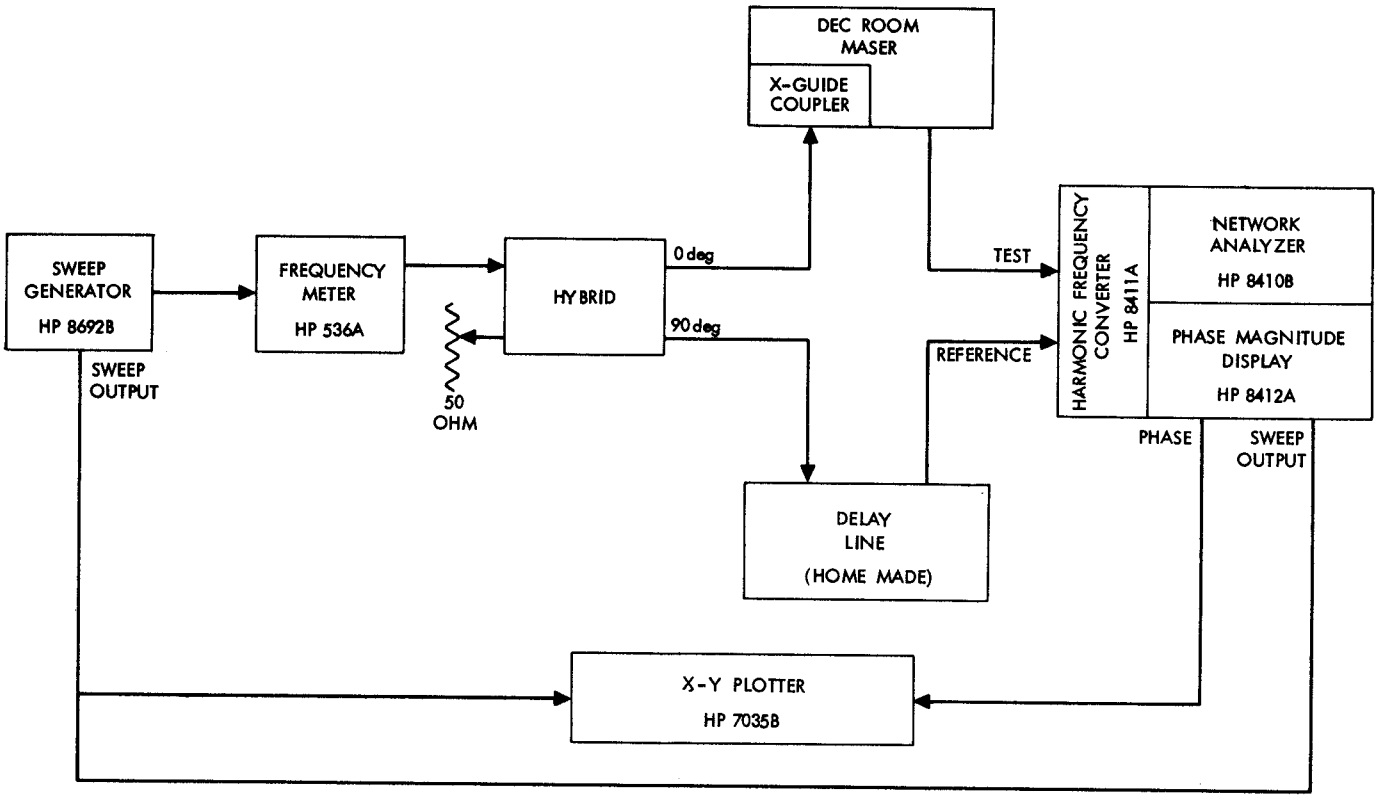

Fig. 2. Test configuration

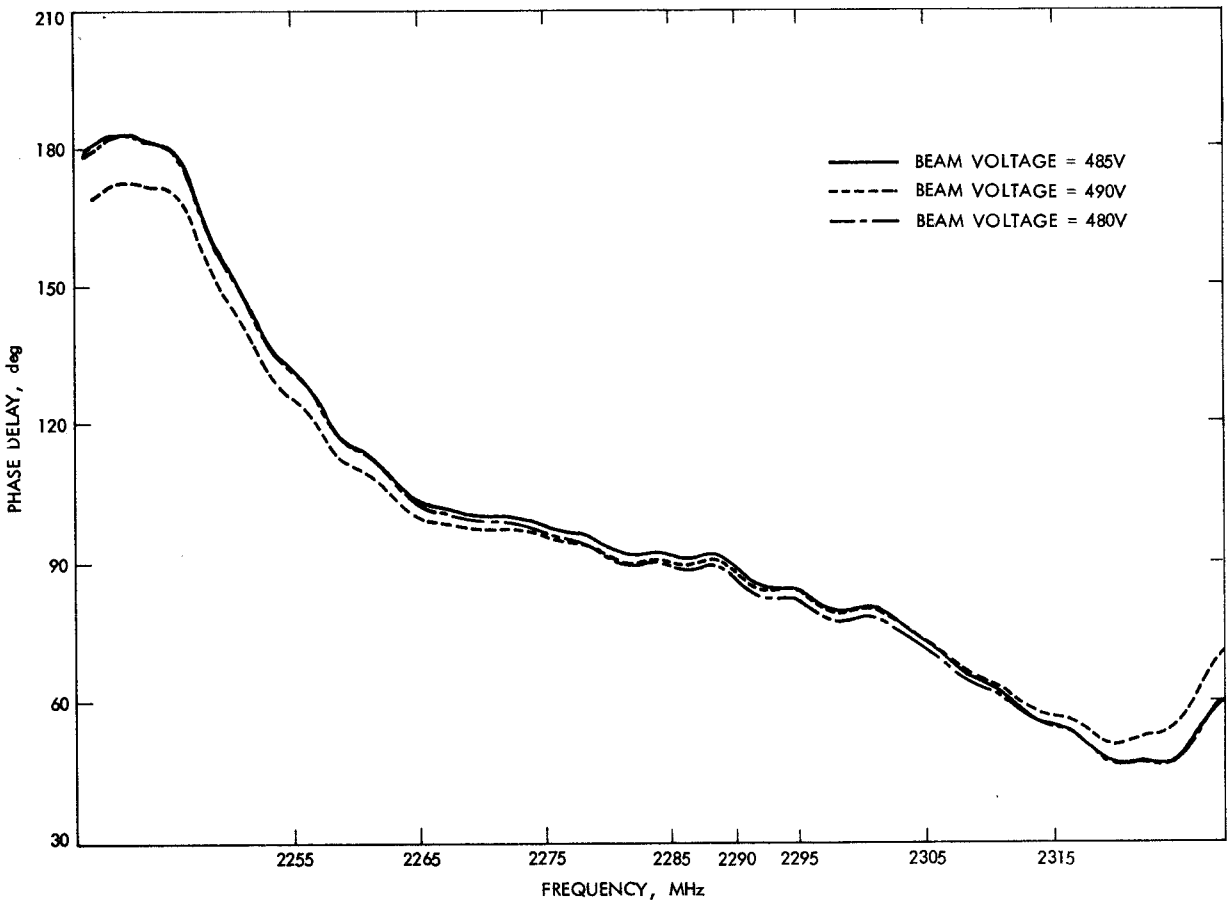

Fig. 3. Phase delay stability vs beam voltage variation

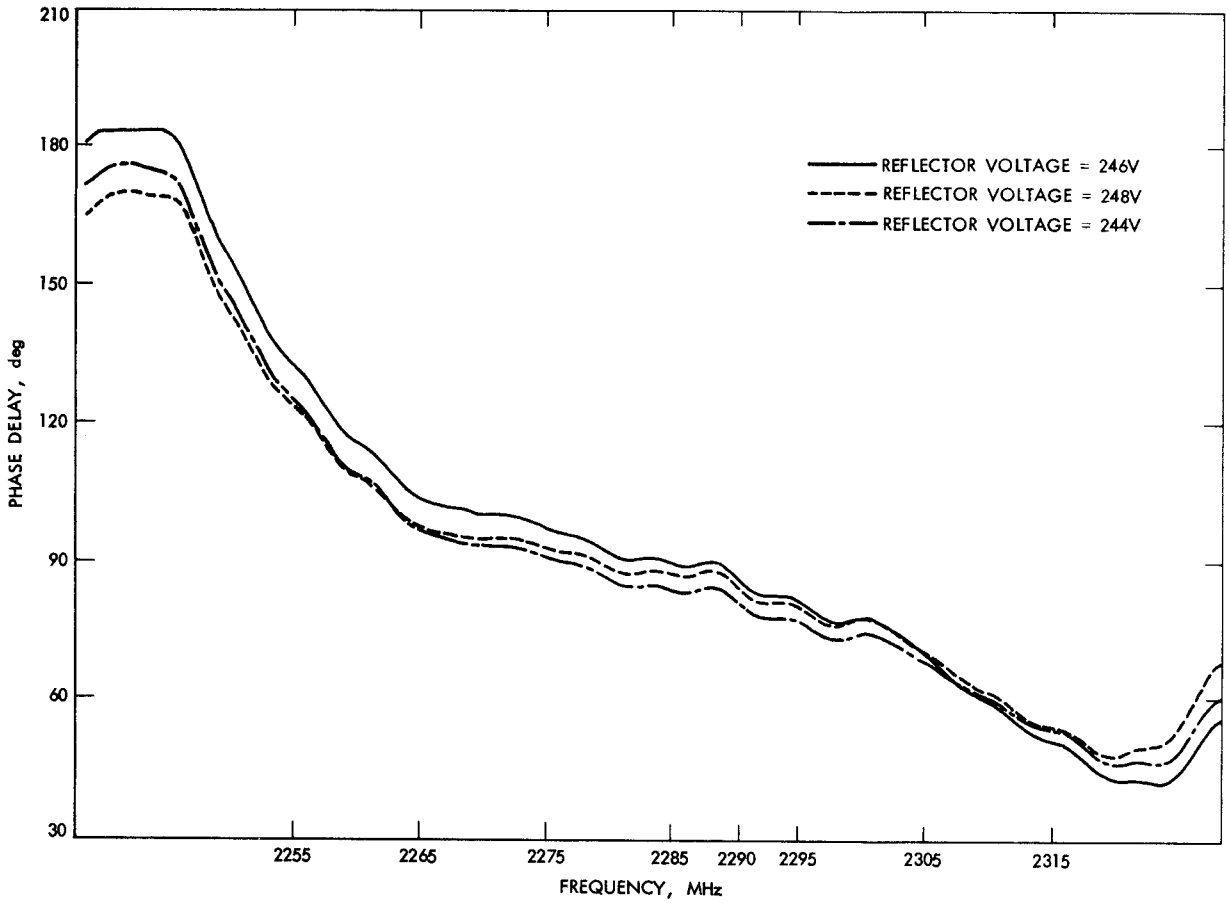

Fig. 4. Phase delay stability vs reflector voltage variation

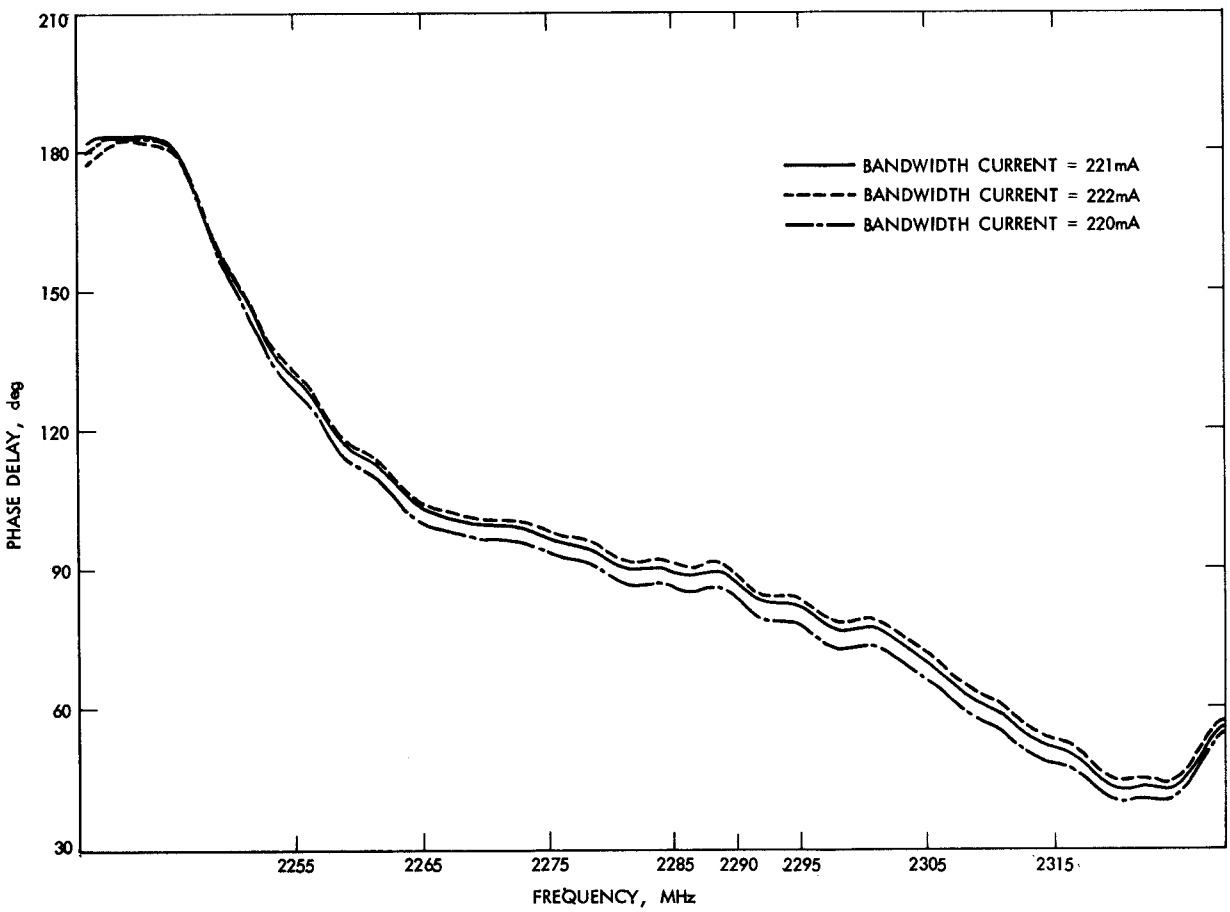

Fig. 5. Phase delay stability vs bandwidth control current variation

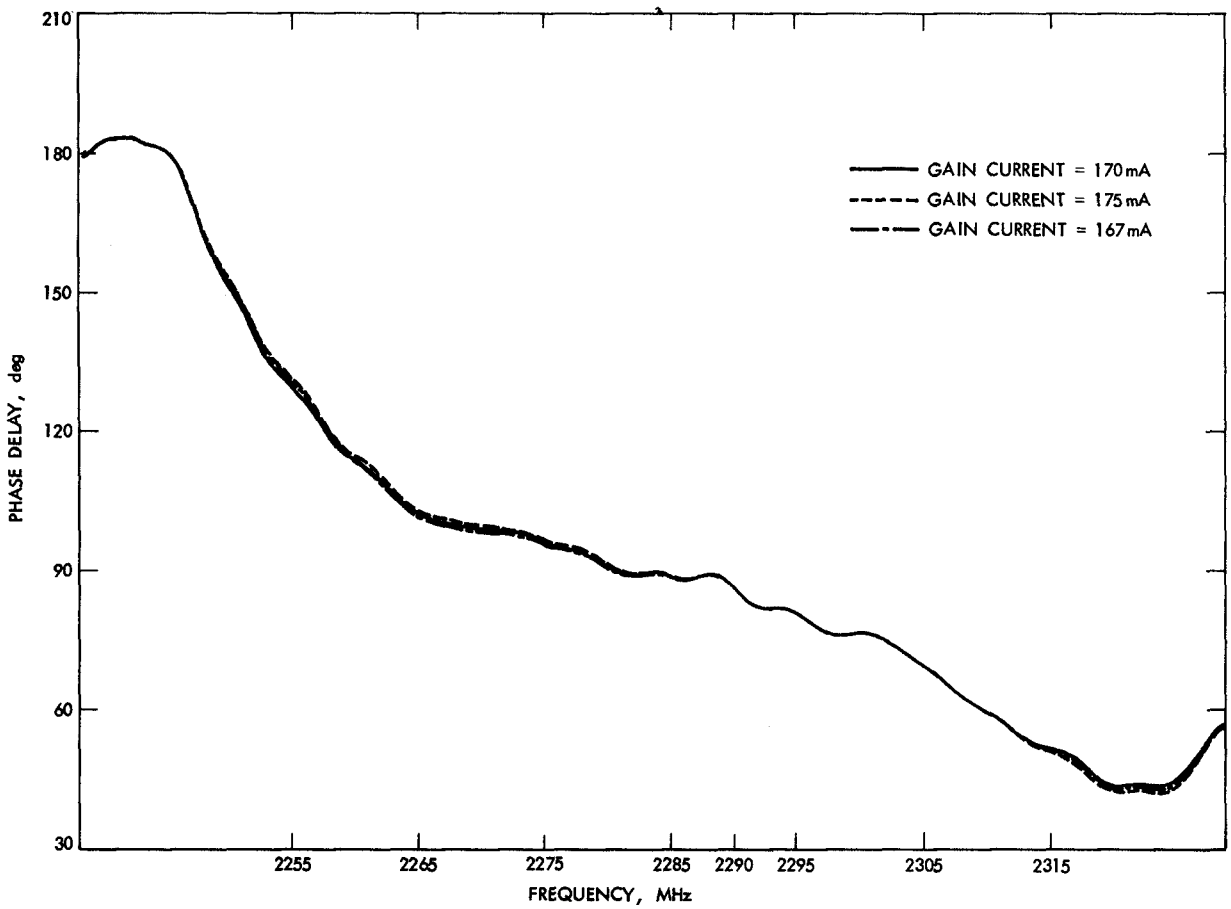

Fig. 6. Phase delay stability vs gain control current variation

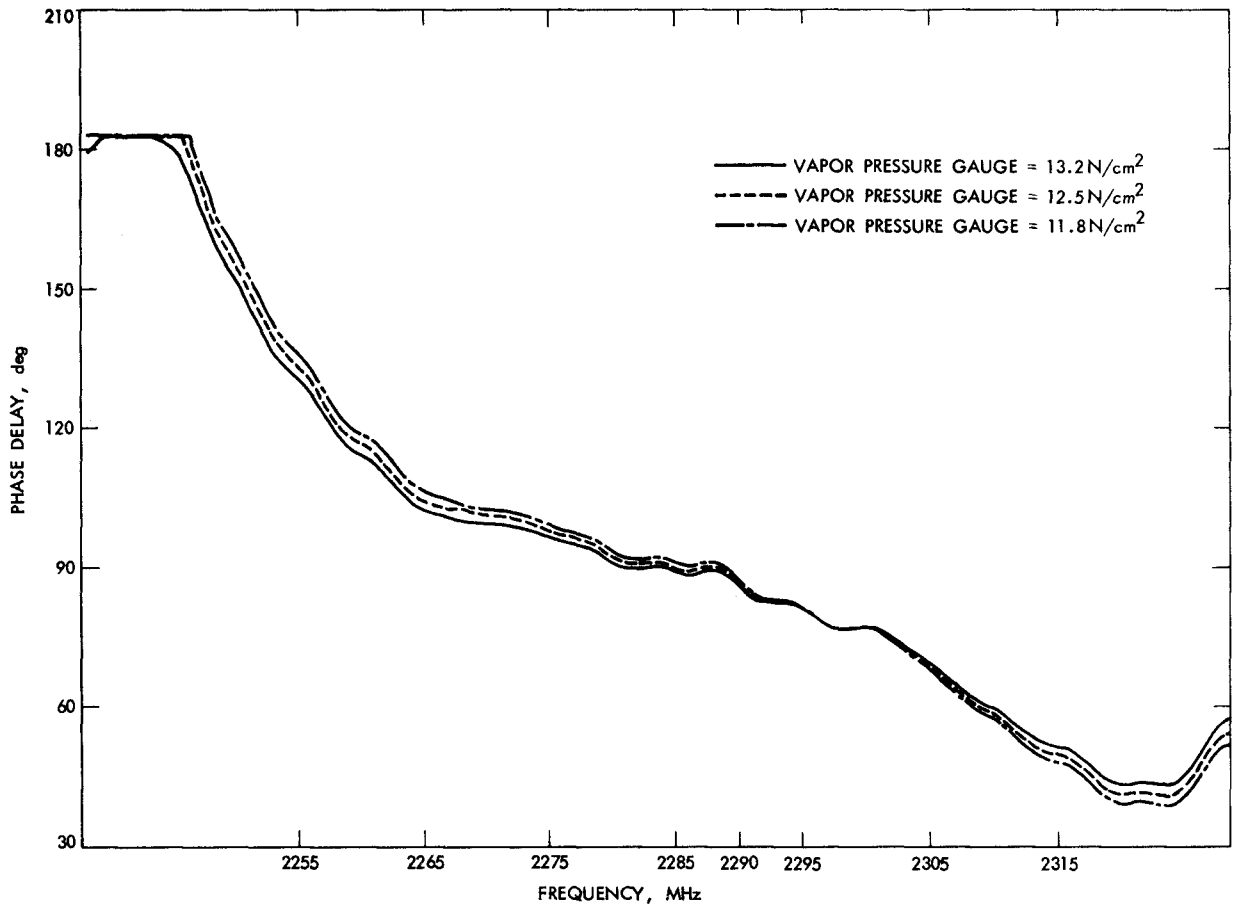

Fig. 7. Phase delay stability vs liquid He temperature

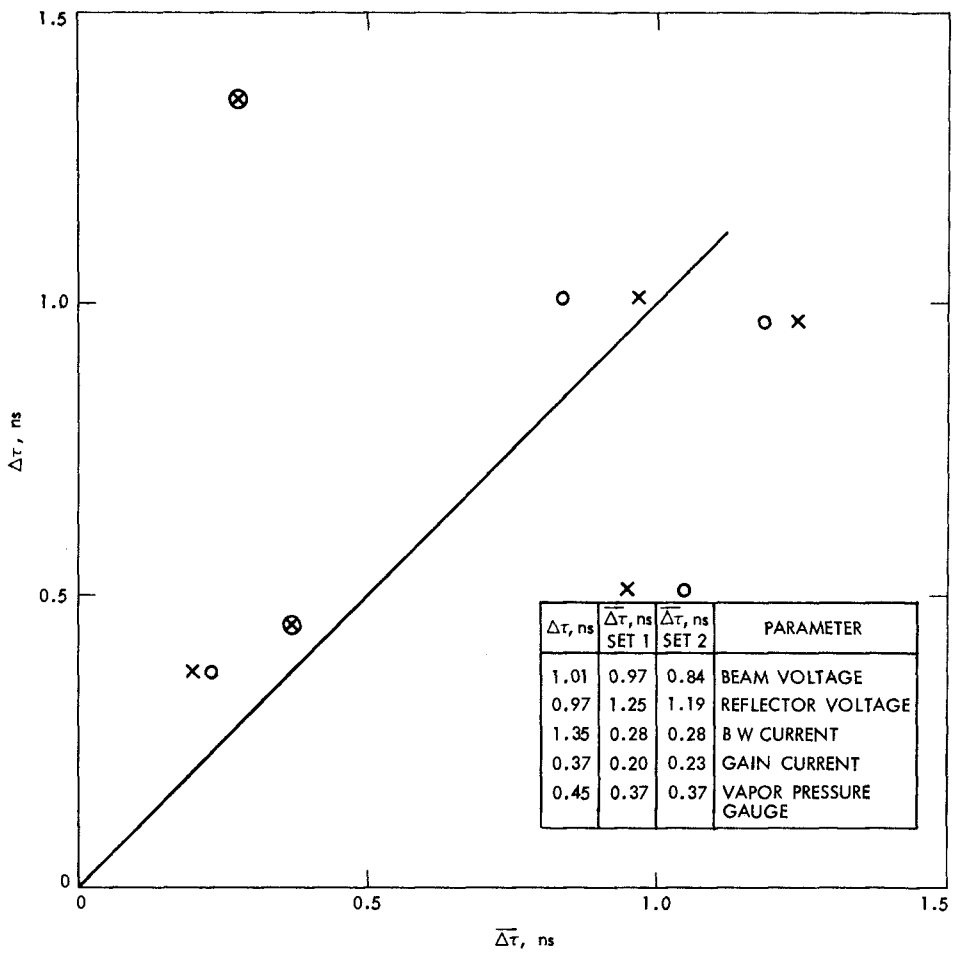

Δτ, ns	$\overline{\Delta\tau}$, ns SET 1	$\overline{\Delta\tau}$, ns SET 2	PARAMETER
1.01	0.97	0.84	BEAM VOLTAGE
0.97	1.25	1.19	REFLECTOR VOLTAGE
1.35	0.28	0.28	B W CURRENT
0.37	0.20	0.23	GAIN CURRENT
0.45	0.37	0.37	VAPOR PRESSURE GAUGE

Fig. 8. Coherency of phase and group delay stability

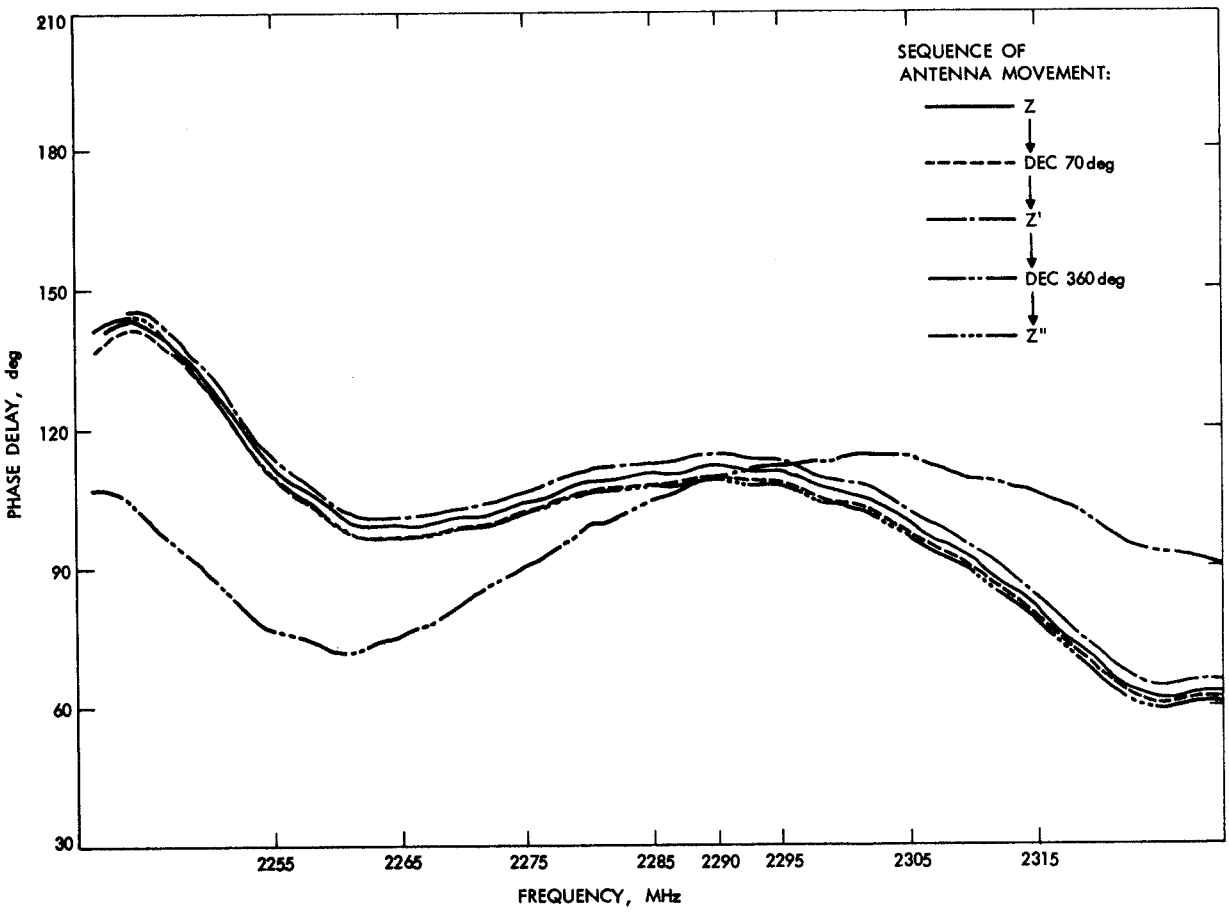

Fig. 9. Phase delay stability vs antenna orientation

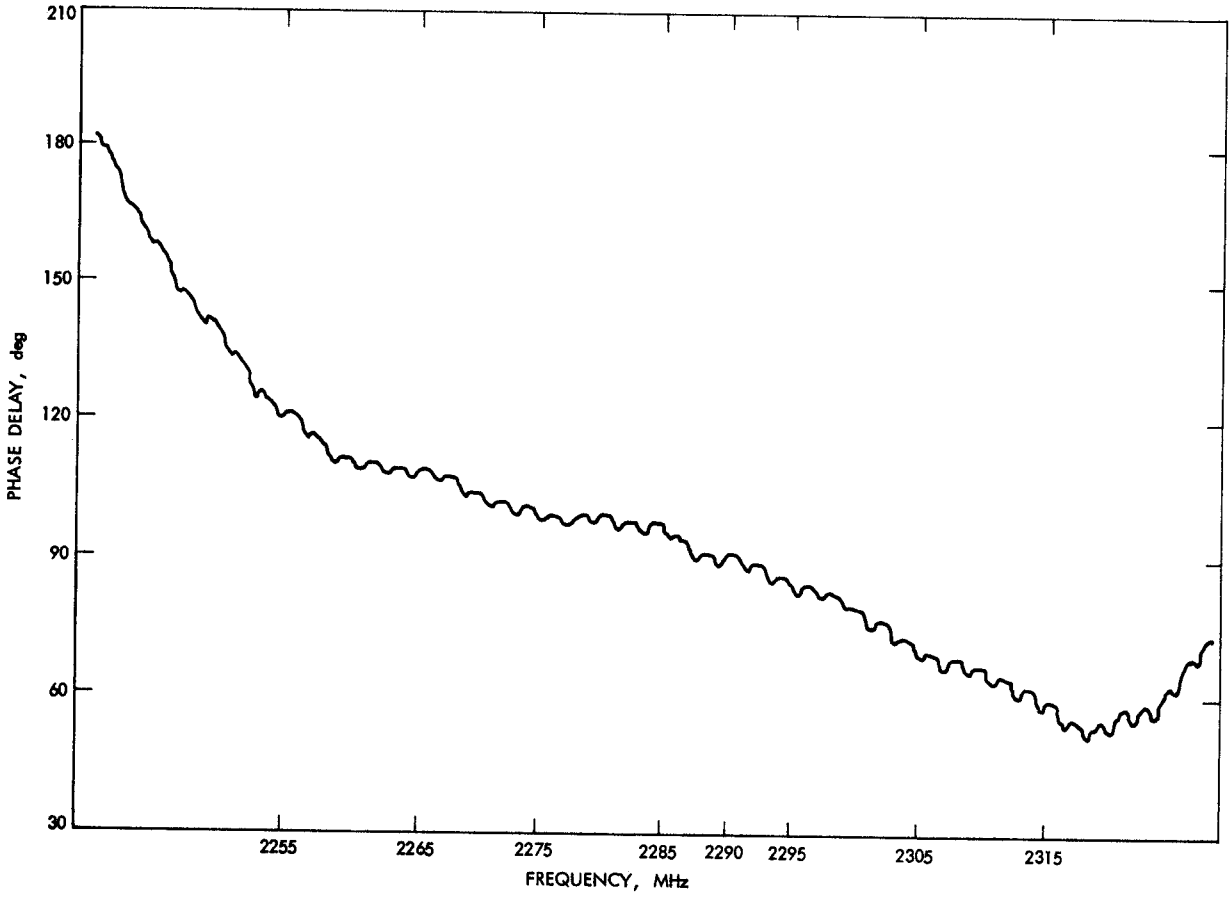

Fig. 10. Cross-head modulation effect on phase delay stability